Supplementary Material

Contribution of physical processes to variability of dissolved silicate in the Labrador Sea between 1980 and 2015.

Alizée Dale[1], Marion Gehlen[1], Douglas W.R. Wallace[2], Germain Bénard[1], Christian Éthé[1], and Elena Alekseenko[3]

[1]Université Paris-Saclay, CNRS, CEA, UVSQ, Laboratoire des sciences du climat et de l'environnement, 91191, Gif-sur-Yvette, France.

[2]Department of Oceanography, Dalhousie University, Halifax, Nova Scotia, B3H 1N4 Canada

[3]Laboratoire d'Océanologie et de Géosciences, CNRS, LOG UMR 8187, 28 Avenue Foch, BP 80, 62930 Wimereux, France

October 30, 2023

Contents of this file

The supporting information presents the evaluation of model output for the Labrador Sea including:

1. the data sets selected for model evaluation (table S1);
2. the evaluation of model output for the Labrador Sea (Fig. S2 to S6 and table S2) ;
3. the external data sets used for model initialization (table S3 and S4);

1 Evaluation of model output for the Labrador Sea

1.1 Selection of period of analysis

The simulation started in 1958 from an ocean at rest. The time series (Fig. S1) of the volume of water integrated between OSNAP and the northern section (upper 450 m) highlights a period of rapid adjustment over the first years followed by a gradual decline to reach a quasi-steady-state from 1980 onwards with a clear seasonal cycle and some low frequency variability.

1.2 Evaluation of surface properties

In addition to the evaluation of simulated and observed dissolved silica (DSi) concentrations along the AR7W section presented in the main section, model output is evaluated hereafter for the Labrador Sea against several additional physical and biogeochemical data sets.

Simulated surface ocean 1981-2010 spring averages (April, May, June) of temperature, practical salinity, and DSi of the Labrador sea are compared in Fig. S2 to corresponding data extracted from the WOA2018. Model output was regridded on the regular WOA grid (1/4° for temperature and salinity, 1° for DSi) prior to model-data comparison.

Modelled distributions of temperature (Fig. S2a) and salinity (Fig. S2b) reflect the surface ocean circulation in the Labrador Sea: inflow of cold and fresh waters from the Arctic which feed the southward flowing Baffin Current along the coast of Baffin Island, inflow of northward-flowing, warm Atlantic waters to the west of Greenland (West Greenland Current, i.e. WGC , West Greenland Slope Current, i.e. WGSC). The signature of the DSi-rich Arctic inflow is seen in the modelled DSi distribution, with a gradient from the Canadian coast towards the center of the basin (Fig. S2c). The model represents colder (Fig. S2d) and fresher (Fig. S2e) waters in the northern part of the domain and along the Canadian coast. Temperature and salinity biases stem from the Arctic inflow and propagate along the coast with the Baffin Current. They are intensified along the east coast of Baffin Island and Labrador Sea. Modelled surface waters are too warm in the north-eastern Labrador Sea and over the WGC , as well as to the south of the domain (offshore Labrador). A mostly small positive salinity bias is found over the same regions. Temperature and salinity biases are small in the center of the Labrador Sea where deep winter convection takes place. A see-saw pattern is found for temperature with, in the model, colder waters to the North and slightly warmer waters to the South. It is associated with a near-zero bias over the same area in salinity. This see-saw pattern south of Greenland (Cape Farewell) mirrors the contrast between the low-salinity WGC (negative bias in temperature) and the warm and salty WGSC [Østerhus et al., 2019]. This reflects the presence of strong contrast between Atlantic (WGC) and Arctic waters (EGC, WGSC) in the model. The concentration of DSi is overestimated over the whole region as discussed in the main text.

1.3 Evaluation along the Davis Strait section

Figure S3 displays cross-sections across Davis Strait for temperature, salinity, and DSi. Data is taken from the September 2004 R/V Knorr cruise (table S1). The bias is computed as the difference between the model's nearest grid point and the observation, and its relative observation point. Temperature and salinity are over-

estimated in the model at the surface and down to approximately 200 m. The positive bias extends deepest at the west of the section, and shallows towards the east. Temperature is underestimated in underlying waters, whereas salinity bias is close to zero. Simulated DSi concentrations are slightly overestimated in the upper 100 meters of the water column and underestimated with depth. Average biases and standard deviations computed over the 0 to 450 m depth layer, the focus of this paper, are: 0.96 ± 0.53°C for temperature, 0.35 ± 0.28 PSU for salinity, and -0.17 ± 1.57 μM for DSi.

1.4 Evaluation of mean vertical profiles

Figure S4 compares the temporal mean (1981-2010) of regionally-averaged profiles of conservative temperature, practical salinity, and DSi concentration between OSNAP and the Northern section as a function of depth. The figures suggest that the model is slightly saltier over the full water column with a maximal bias of 0.25 PSU at the surface. Bias in temperature is maximal at the surface (+1.3°C in the model) and minimal at 1600 m (+0.05°C). The mean temperature is overestimated in the model from the surface down to 1500 m and below 3000 m. It agrees with observations between 1500 m and 3000 m. Modelled DSi concentrations agree well with WOA2018 data until 50 m of depth. The model underestimates DSi concentration down to 2000 m of depth. Below 2000 m, modelled DSi concentrations are overestimated. The overestimation of DSi at depth likely reflects a too large contribution of Antarctic Bottom Waters (AABW) rich in DSi along with an underestimation of dense overflows from the Nordic seas.

1.5 Evaluation of DSi interannual variability and trends

This section complements section 3.1 and figure 1b of the main text. It (i) provides the absolute values of DSi concentration across the AR7W section in the model and observation datasets, (ii) highlights the statistical relationship between the observations and the model concentration, and (iii) shows the spatial differences between the model and the observations along the section.

The linear regression has a slope of 0.58 with R^2 = 0.71 (p-value $<$ 0.01; Fig. S5b). Hence the model dynamics explain 82 $\%$ of the variance of the observations. The variability in DSi concentration is concentrated in the first 200 km of the section (i.e., its western edge; Fig. S5c) in the observations while it is focused on the eastern part of the section in the model.

1.6 Evaluation of Mixed Layer Depth

The yearly mean MLD (Fig. S6a) is underestimated over most of the domain, with a notable exception in the center of the Labrador Sea, where modelled MLDs exceed those observed by up to 330 m (Fig. S6b). The region-wide bias stems from underestimating winter MLDs when MLD peaks and deepwater convection occurs (Fig. S6c). The density criterion used to define the MLD could be responsible for the overestimation at the center of the Labrador sea in the model. According to [Courtois et al., 2017], it is not the most suitable criterion during strong deep convection events as it is subject to temperature-salinity compensation leading to the overestimation by the model. It could be better to use a temperature or salinity-based method [Courtois et al., 2017]. However, the winter-time deep convection location in the model seems to be in agreement with the observations.

The annual maximum MLD in the model is compared to the annual maximum MLD observation-based estimates from [Yashayaev and Loder, 2016] over the same region (Fig. S6d). Observations show a gradual decrease in maximum MLD from 1994 onwards whereas the model shows a sharp drop in MLD between 1994 and 1995, followed by a period of low values and low variability. Until 2007, the annual maximum MLD decreased by - 29.6 m/y (p-value $<$ 0.03). MLD extrema in the model and the observations do not always coincide. In addition, the model exhibits variability on the 2-4 years time scale of relatively high magnitude compared to the observations. The observed MLD decreases linearly at a rate of -114.5 m/yr (p-value $<$ 0.01) between 1994 and 2007. This contrasts with the model which exhibits high amplitude interannual variability, particularly a sharp drop between 1993 and 1995.

1.7 Evaluation of the transport across Davis Strait, the Northen section and OSNAP

Simulated net volume and DSi transports were computed along the Northern section and OSNAP sections, and are compared to data-based assessments in Table S2. Net volume transports (integration of the Eulerian velocity and the eddy-induced velocity) are computed online at the temporal resolution of the ocean general circulation model (900 sec) before monthly averaging. DSi transport was computed off-line as the product of the monthly net transport rates and monthly DSi concentrations. While the simulated volume transport across the Northern section is coherent with the long-term mean estimate (2004-2010) of [Curry et al., 2014], it is only half of that used by [Torres-Valdés et al., 2013] for summer 2005 (1.6 ± 0.2 Sv across the Northern section in the model). While the volume transport varies seasonally, with a maximum reached in summer due to the contribution of ice melt [Curry et al., 2014], the difference between the long-term mean and the summer estimates exceeds the range of seasonal variability. [Torres-Valdés et al., 2013]

derived velocities for volume and tracer transports from an inverse box model representing the Arctic Ocean, which is different from the approach taken in this study and is likely to contribute to the difference in volume transport. The difference in volume transport between this study and that of [Torres-Valdés et al., 2013] across the Davis Strait is also found in DSi transport. Combining the volume transport and the DSi transport from [Torres-Valdés et al., 2013], we compute an average DSi concentration of 13.8 μM in waters crossing the Davis Strait, which is only slightly higher than in the model (12.3 μM).

At OSNAP, the simulated net volume transport between 1980 and 2015 exceeds that at the northern boundary by 0.1 Sv, while being within the estimate by [Lozier et al., 2019] for the 2004-2010 long term mean. Modelled mean net volume transports across the two sections fall within the range of standard deviations of independent estimates. A slightly higher transport across OSNAP is expected due to the contribution of water leaving the Canadian Arctic Archipelago through the Hudson Strait.

Table S1: Main characteristics of observation-based products used for model evaluation. [a]The MLD is based on a density difference with respect to the surface of 0.01 kg/m3.

Products	Variables	Time scale	Source
R/V Knorr cruise at Davis Strait	Temperature, Salinity, DSi, NO_3^-	2004	[Lee et al., 2004] https://cchdo.ucsd.edu/cruise/316N20040922
Combination of Argo data and mooring CTD processed at the BIO	MLD[a]	1980-2017	[Yashayaev and Loder, 2016, Raimondi et al., 2021]
World Ocean Atlas 2018 Reanalysis (WOA2018)	Temperature, salinity, DSi, NO_3^-, PO_4 and MLD[a]	1981-2010 mean	[Boyer et al., 2018] https://www.ncei.noaa.gov/

Table S2: Net volume and DSi transports across Davis Strait, the Northen section and OSNAP.

Mean ± SD	Northern section for model output/Davis Strait for data		OSNAP	
Sources	**Net volume transport (Sv)**	**Net DSi transport (kmol/s)**	**Net volume transport (Sv)**	**Net DSi transport (kmol/s)**
Model Long term mean 1980-2015	NS: -1.6 ± 0.7	NS: -18.8 ± 5.9	-1.7 ± 0.7	-17.6 ± 12.3
[Torres-Valdés et al., 2013] Summer 2005	-3.1 ± 0.3	-42.9 ± 5.2	NA	NA
[Curry et al., 2014] Long term mean 2004-2010	-1.6 ± 0.2	NA	NA	NA
[Lozier et al., 2019] Long term mean 2004-2010	[Curry et al., 2014]	NA	-1.6 ± 0.2	NA
Model Long term mean 2004-2010	NS: -1.4 ± 0.7	NS: -15.01 ± 4.3	-1.4 ± 0.7	-11.3 ± 11.3

Table S3: Characteristics of model initialization

Elements	**Sources**
Conservative Temperature, Absolute salinity	World Ocean Atlas 2013 [Locarnini et al., 2013]
Nitrate, Silicate, Phosphorus and Oxygen	World Ocean Atlas 2009 [Garcia et al., 2009]
Iron and DOC	PISCES outputs [Aumont et al., 2015]
Alkalinity	Glodap v2 [Olsen et al., 2016]
DIC	Glodap Pre-industrial DIC [Lauvset et al., 2016]

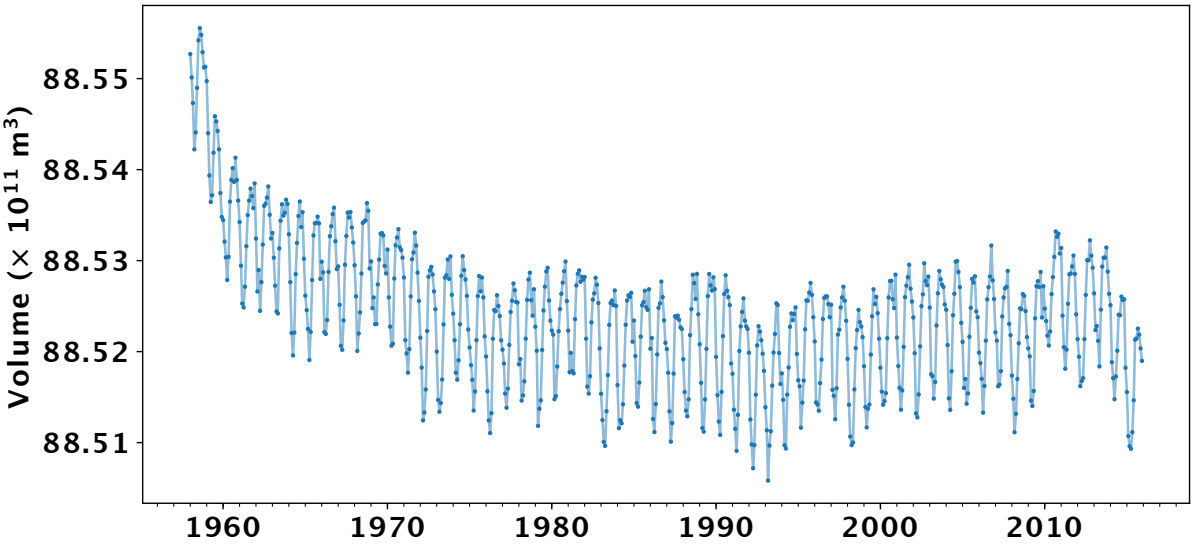

Figure S1: Monthly averaged volume of water integrated over the first 450 m between OSNAP and the Northern section.

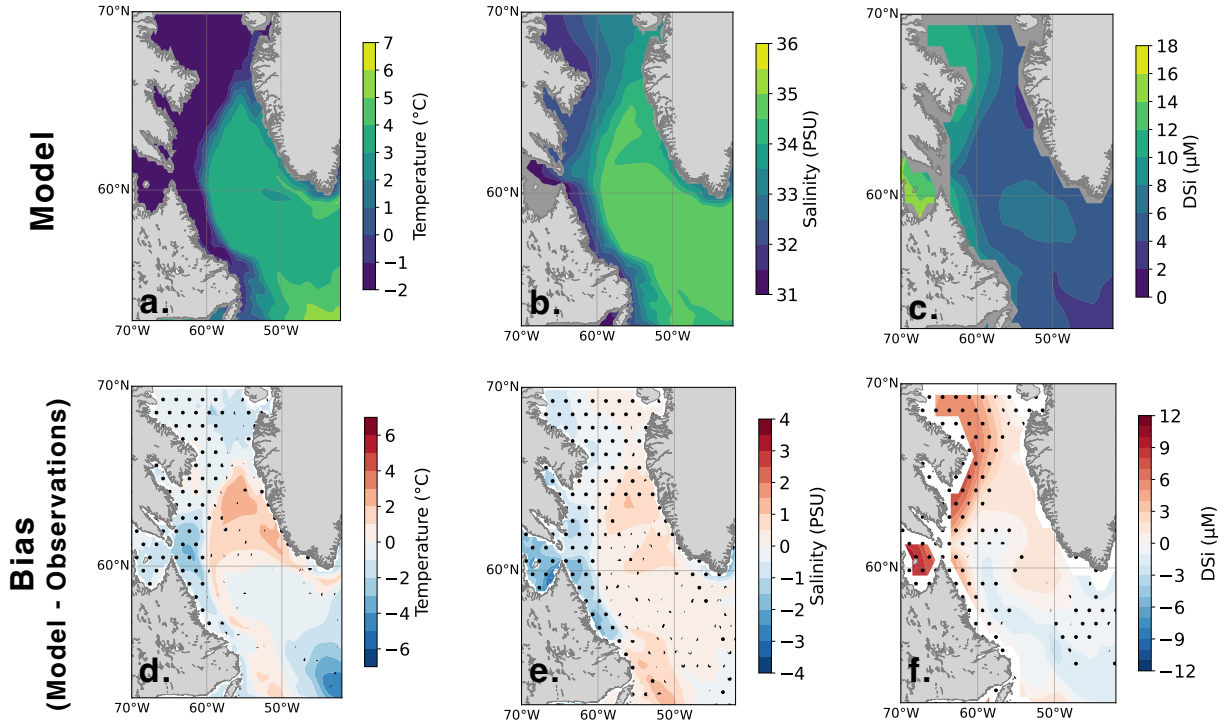

Figure S2: Surface ocean averages for spring (AMJ) of conservative temperature (°C), salinity (PSU), and DSi concentration (μM). (a) to (c) model output, (d) to (f) average biases between model output and WOA2018. Temperature and salinity data from the WOA2018 dataset have a 1/4° resolution, and DSi has a 1° resolution. Model outputs have been remapped on the WOA2018 grid for both sets of figures. Stippling highlight field interpolation area, i.e. areas where observations are absent.

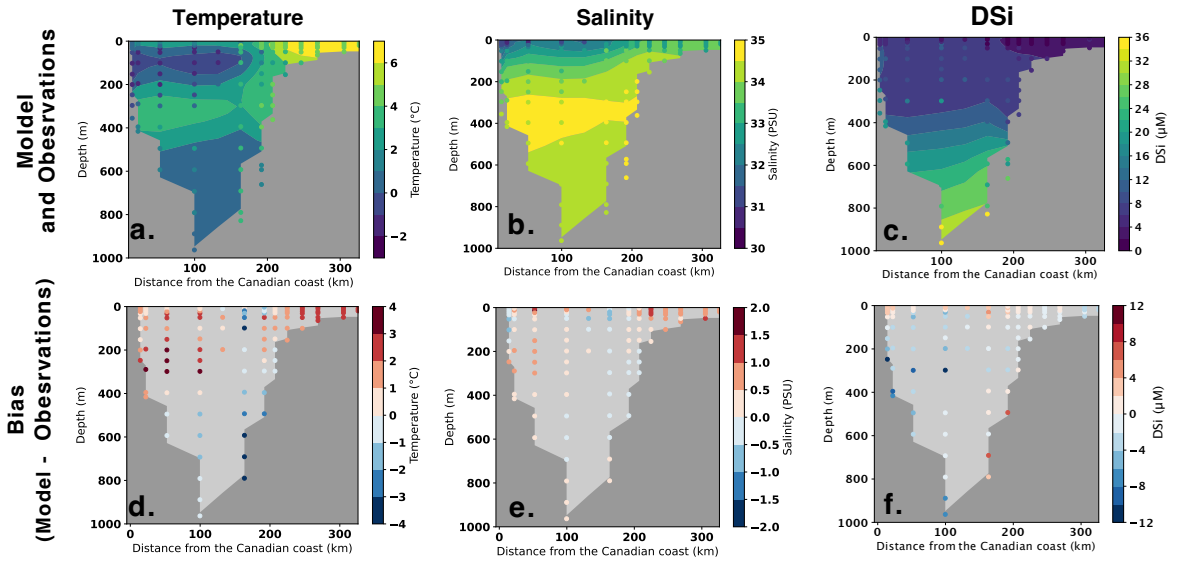

Figure S3: Comparison of model output and observations for (a) temperature, (b) salinity, and (c) DSi along Davis Strait in September 2004. Modelled distributions are displayed as colored fields with discrete samples overlain as dots (same color scale). Panels (d) to (f) show the bias (model – observations) after co-localizing model output on the model grid.

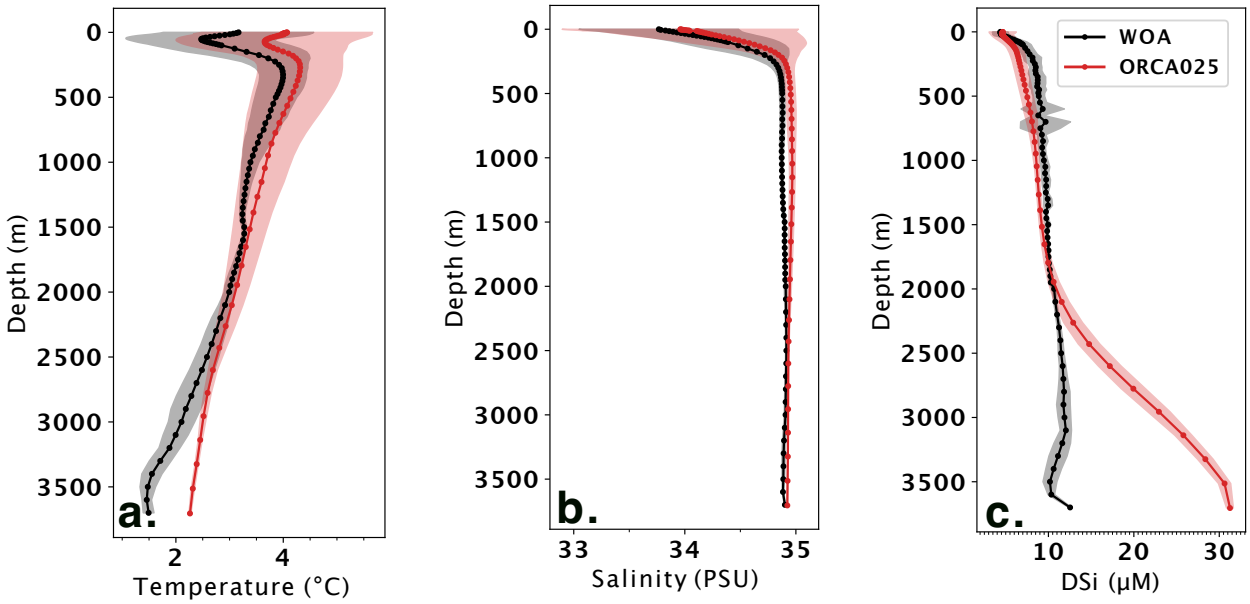

Figure S4: Mean vertical profiles for the period 1981-2010 of: (a) temperature, (b) salinity, and (b) DSi concentration averaged between the OSNAP section and the Northern section. Observational data from the WOA2018 dataset are shown with black lines and shading; model output is represented with red lines and shading. The shaded area represents one standard deviation.

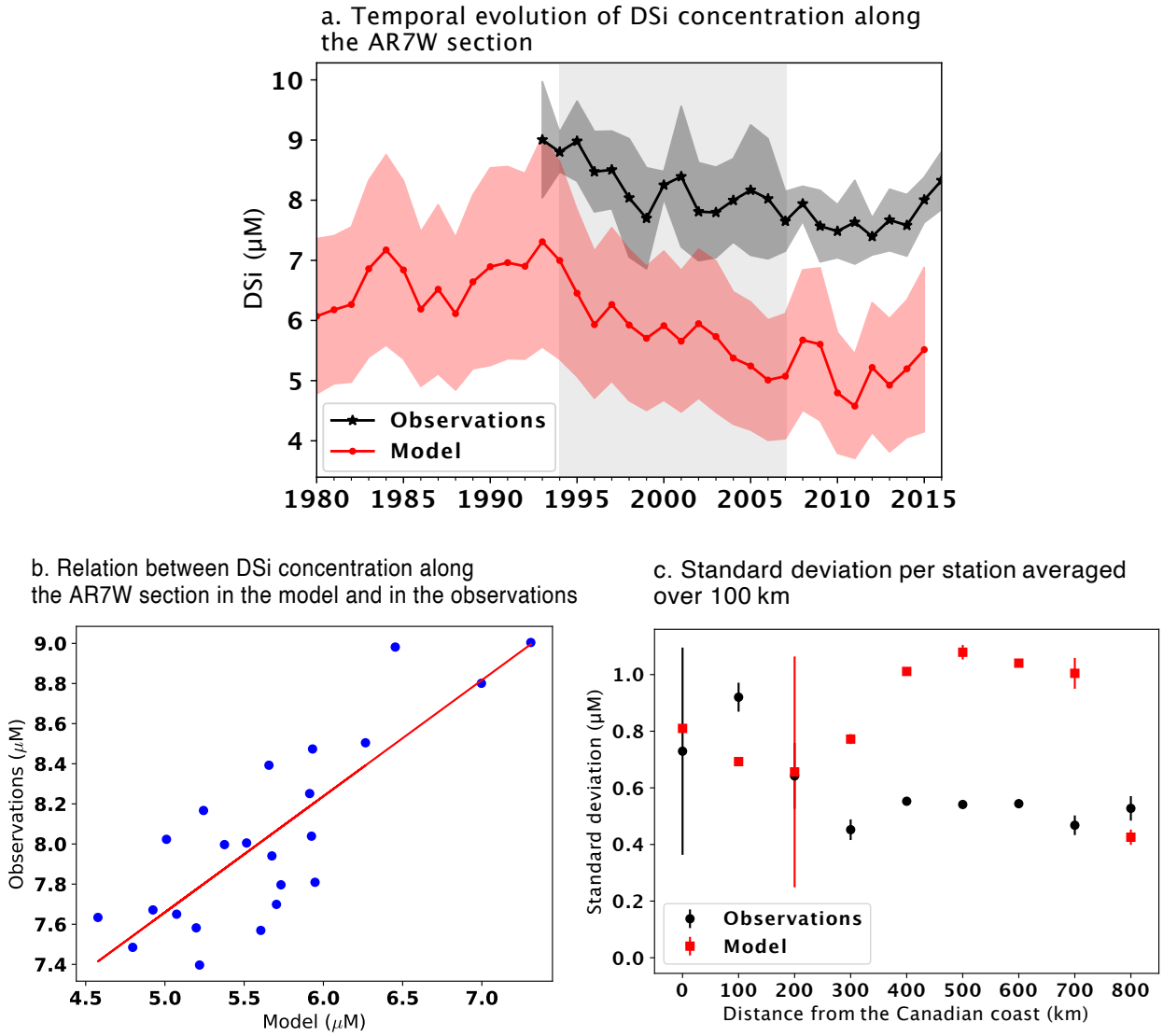

Figure S5: Evolution of AR7W DSi concentration from the observation-based data and in the model. a. Temporal evolution of DSi concentration of the upper 450 m along the AR7W section as observed and simulated in ORCA025. The average bias is 2.3 μM (see main text) b. Relation between DSi concentration along the AR7W section in the model and the observations.

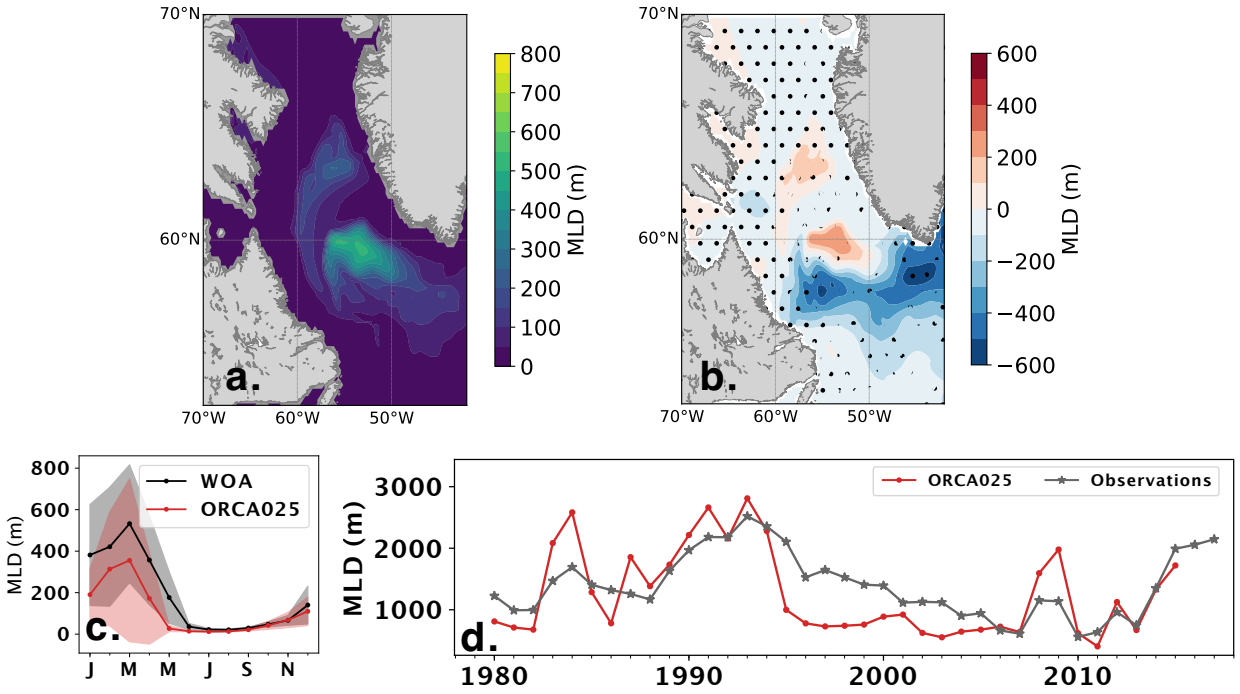

Figure S6: Evaluation of modelled Mixed Layer Depth over the period from 1980 to 2010: (a) average MLD in the model after remapping on the regular WOA2018 grid (1/4° resolution); (b) bias (model – data) between modelled and observed mean MLD ; (c) seasonal cycle of mean MLD (solid lines, red for model and black for WOA), shading represents the spatial standard deviation for the region between OSNAP and the study area's northern boundary ; (d) time series of annual maximum MLD in the Labrador Sea from the observation-based values derived by Yashayaev and Loder (2016) (gray), and from the model (red).

Table S4: List of PISCES external inputs adaptated from Aumont et al. (2015)

Inputs	**Elements**	**Sources**
Dust deposition	Fe, Si, P	LMDZOR-INCA chemistry model [Boucher et al., 2020, Lurton et al., 2020]
Nitrogen deposition	N	NCAR (https://esgf-node.llnl.gov/projects/input4mips/)
River supply	all elements	GLOBAL NEWS2 data set [Mayorga et al., 2010]

References

[Aumont et al., 2015] Aumont, O., Éthé, C., Tagliabue, A., Bopp, L., and Gehlen, M. (2015). Pisces-v2: an ocean biogeochemical model for carbon and ecosystem studies. *Geoscientific Model Development Discussions*, 8(2).

[Boucher et al., 2020] Boucher, O., Servonnat, J., Albright, A. L., Aumont, O., Balkanski, Y., Bastrikov, V., Bekki, S., Bonnet, R., Bony, S., Bopp, L., et al. (2020). Presentation and evaluation of the ipsl-cm6a-lr climate model. *Journal of Advances in Modeling Earth Systems*, 12(7):e2019MS002010.

[Boyer et al., 2018] Boyer, T. P., García, H. E., Locarnini, R. A., Zweng, M. M., Mishonov, A. V., Reagan, J. R., Weathers, K. A., Baranova, O. K., Paver, C. R., Seidov, D., et al. (2018). World ocean atlas.

[Courtois et al., 2017] Courtois, P., Hu, X., Pennelly, C., Spence, P., and Myers, P. G. (2017). Mixed layer depth calculation in deep convection regions in ocean numerical models. *Ocean Modelling*, 120:60–78.

[Curry et al., 2014] Curry, B., Lee, C., Petrie, B., Moritz, R., and Kwok, R. (2014). Multiyear volume, liquid freshwater, and sea ice transports through davis strait, 2004–10. *Journal of Physical Oceanography*, 44(4):1244–1266.

[Garcia et al., 2009] Garcia, H., Locarnini, R., Boyer, T., Antonov, J., Zweng, M., Baranova, O., and Johnson, D. (2009). World ocean database 2009, vol 4: nutrients (phosphate, nitrate, silicate). *US government printing office, Washington, DC*.

[Lauvset et al., 2016] Lauvset, S. K., Key, R. M., Olsen, A., Van Heuven, S., Velo, A., Lin, X., Schirnick, C., Kozyr, A., Tanhua, T., Hoppema, M., et al. (2016). A new global interior ocean mapped climatology: The 1×1 glodap version 2. *Earth System Science Data*, 8(2):325–340.

[Lee et al., 2004] Lee, C. M., Petrie, B., Gobat, J. I., Soukhovtsev, V., and Abriel, J. (2004). An observational array for high-resolution, year-round measurements of volume, freshwater, and ice flux variability in davis strait: Cruise report for r/v knorr 179-05, 22 september-4 october 2004. Technical report, WASHINGTON UNIV SEATTLE APPLIED PHYSICS LAB.

[Locarnini et al., 2013] Locarnini, R., Mishonov, A., Antonov, J., Boyer, T., Garcia, H., Baranova, O., Zweng, M., Paver, C., Reagan, J., Johnson, D., et al. (2013). World ocean atlas 2013, volume 1: Temperature, edited by: Levitus, s. *A. Mishonov Technical Ed., NOAA Atlas NESDIS*, 73:40.

[Lozier et al., 2019] Lozier, M. S., Li, F., Bacon, S., Bahr, F., Bower, A. S., Cunningham, S., de Jong, M. F., de Steur, L., deYoung, B., Fischer, J., et al. (2019). A sea change in our view of overturning in the subpolar north atlantic. *Science*, 363(6426):516–521.

[Lurton et al., 2020] Lurton, T., Balkanski, Y., Bastrikov, V., Bekki, S., Bopp, L., Braconnot, P., Brockmann, P., Cadule, P., Contoux, C., Cozic, A., et al. (2020). Implementation of the cmip6 forcing data in the ipsl-cm6a-lr model. *Journal of Advances in Modeling Earth Systems*, 12(4):e2019MS001940.

[Mayorga et al., 2010] Mayorga, E., Seitzinger, S. P., Harrison, J. A., Dumont, E., Beusen, A. H., Bouwman, A., Fekete, B. M., Kroeze, C., and Van Drecht, G. (2010). Global nutrient export from watersheds 2 (news 2): model development and implementation. *Environmental Modelling & Software*, 25(7):837–853.

[Olsen et al., 2016] Olsen, A., Key, R. M., Van Heuven, S., Lauvset, S. K., Velo, A., Lin, X., Schirnick, C., Kozyr, A., Tanhua, T., Hoppema, M., et al. (2016). The global ocean data analysis project version 2 (glodapv2)–an internally consistent data product for the world ocean. *Earth System Science Data*, 8(2):297–323.

[Østerhus et al., 2019] Østerhus, S., Woodgate, R., Valdimarsson, H., Turrell, B., De Steur, L., Quadfasel, D., Olsen, S. M., Moritz, M., Lee, C. M., Larsen, K. M. H., et al. (2019). Arctic mediterranean exchanges: A consistent volume budget and trends in transports from two decades of observations. *Ocean Science*, 15(2):379–399.

[Raimondi et al., 2021] Raimondi, L., Tanhua, T., Azetsu-Scott, K., Yashayaev, I., and Wallace, D. W. (2021). A 30-year time series of transient tracer-based estimates of anthropogenic carbon in the central labrador sea. *Journal of Geophysical Research: Oceans*, 126(5):e2020JC017092.

[Torres-Valdés et al., 2013] Torres-Valdés, S., Tsubouchi, T., Bacon, S., Naveira-Garabato, A. C., Sanders, R., McLaughlin, F. A., Petrie, B., Kattner, G., Azetsu-Scott, K., and Whitledge, T. E. (2013). Export of nutrients from the arctic ocean. *Journal of Geophysical Research: Oceans*, 118(4):1625–1644.

[Yashayaev and Loder, 2016] Yashayaev, I. and Loder, J. W. (2016). Recurrent replenishment of l abrador s ea w ater and associated decadal-scale variability. *Journal of Geophysical Research: Oceans*, 121(11):8095–8114.